

Synthetic Resampling Methods for Variance Estimation in Parametric Images

Ranjan Maitra

Statistics and Data Mining Research Group
Bellcore, Morristown NJ 07960, USA *

Abstract. Parametric imaging procedures offer the possibility of comprehensive assessment of tissue metabolic activity. Estimating variances of these images is important for the development of inference procedures in a diagnostic setting. Unfortunately, the complexity of the radio-tracer models used in the generation of a parametric image makes analytic variance expressions intractable. A natural extension of the usual resampling approach is infeasible because of the computational effort. This paper suggests a computationally practical approximate simulation strategy to variance estimation. Results of experiments done to evaluate the approach in a simplified model one-dimensional problem are very encouraging. The suggested methodology is evaluated here in the context of parametric images extracted by mixture analysis; however, the approach is general enough to extend to other parametric imaging methods.

1 Introduction

The ability to assess quantitatively the biologic status of tissue from a sequence of dynamic Positron Emission Tomography (PET) scans is one of the most powerful features of this radiologic tool. The most common approach in this regard is a technique called ROI analysis. Here, the reconstructed pixel values in each scan are averaged over a given region (ROI) to yield a time series, called the *time-activity curve* (TAC), and then the regional biologic parameter values are estimated by fitting non-linear models to the time series. There are concerns regarding image registration while drawing these regions with the help of other imaging modalities such as X-ray Computed Tomography (CT) or Magnetic Resonance Imaging (MRI), as well as the potential for inaccurate metabolic parameter estimation because of the possible selection of inhomogeneous regions [22]. From a practical standpoint however, the most important concern is that outside the selected regions, the reconstructed PET data are only interpreted qualitatively, thus compromising the quantitative potential of this expensive technology.

Parametric imaging attempts to offer comprehensive pixel-wise assessments of tissue metabolic activity. The technique builds on fitting radio-tracer models to the time-course reconstructed PET data at each pixel. However, the presence of noise and heterogeneity between the reconstructed pixel values makes

* Research supported in part by the National Institutes of Health grant CA-57903 at the University of Washington, Seattle, USA.

direct fitting of models inappropriate [12, 24], and underlines the need for more refined approaches (Blomqvist [1], Cunningham and Jones [4], Gjedde [9, 10], Herholz [13], Patlak, *et al.* [23], O’Sullivan [20, 22]).

The full quantitative potential of PET can be realized if it is possible to draw scientific inferences from these parametric images. To this end, in recent years, there has been considerable attention directed to the analysis of multi-subject cerebral activation studies using [O-15]-water [8, 26]. Such studies are interesting in determining, for instance, how the brain processes different cognitive tasks and functions. However, in a clinical setting, there is a practical need for inference tools to guide diagnostic decisions from single-patient studies [14, 15]. In this context, Blomqvist *et al.* [2] noted the desirability of developing methodology to estimate variances in parametric images. Such mechanisms will permit the evaluation of hypotheses related not only to the mean parameter over regions but also regional heterogeneity measures. The statistical significance of any hypothesis test is based on the assumption that under the null hypothesis, the behavior of the test statistic can be explained in terms of purely random variation. In setting up such a test, estimates of dispersion are needed. Unfortunately however, the nonlinear formulations used in the construction of parametric images make analytic variance formulae intractable. The simulation approach of Haynor and Woods [11] could theoretically be extended to develop a variation of the bootstrap method of Efron [6]. This would involve simulating inhomogeneous Poisson processes, independent over time, in the observation (sinogram) domain with (time-dependent) mean intensities estimated by the count data, applying image reconstruction and parametric image generation to obtain an ensemble of simulated functional images. The resampled parametric images could then be used to estimate the dispersions. Unfortunately, the cumulative computational burden of the number of reconstruction steps needed in the simulation makes such an approach impractical.

This paper suggests a synthetic simulation approach via the parametric bootstrap [6] executed in the imaging domain. Under idealized projection conditions, each reconstructed PET scan is well approximated by a multivariate Gaussian distribution. The mean of this distribution is estimated by the reconstructed image. Computationally feasible and accurate dispersion estimates developed in Maitra and O’Sullivan [16, 19] and Maitra [17, 18] are exploited and the result validated for a realistic range of total expected counts. This model is used to simulate dynamic PET sequences, from each of which biologic parameters are extracted. This yields a bootstrap sample of the functional images, which can be used to assess variability. The advantage of this approach over the one that extends the strategy in [11] is that it eliminates the computationally expensive reconstruction step when simulating from the observation process.

The main contributions of this paper are presented in two sections. Section 2 develops the methodology used in the simulation of dispersion estimates. Section 3 reports on the experiments done to validate the approximate Gaussian distributional assumption of reconstructed PET scans, as well as those done to assess the performance of the suggested methodology. Since the latter is not possible

to evaluate in a two-dimensional PET setup, the suggestions are evaluated on experiments performed on a model one-dimensional problem with reconstruction characteristics similar to PET. Finally, Section 4 summarizes the contributions of this paper and poses questions for future research.

2 Theory and Methods

2.1 Distribution of a Time-course Reconstructed PET Sequence

The reconstruction algorithm in PET for the distribution of radio-tracer in tissue at a fixed time-point is the filtered backprojection algorithm:

$$\hat{\lambda}_i^h = \sum_{\theta=1}^{n_\theta} \sum_{d=1}^{n_d} e_h(u_i \cos \theta + v_i \sin \theta - d)y_{d,\theta}. \quad (1)$$

Here $y = \{y_{d,\theta}; d = 1, 2, \dots, n_d; \theta = 1, 2, \dots, n_\theta\}$ is the corrected sinogram data, $e_h(\cdot)$ is the reconstruction filter with resolution size (FWHM) h , $\lambda = \{\lambda_i; i = 1, 2, \dots, I\}$ is the source distribution and $\hat{\lambda}^h$ the corresponding reconstruction.

Theoretically, it can be shown that the asymptotic distribution of the reconstructed PET scan at a fixed time-point under idealized projection conditions is multi-Gaussian [17, 18]. The mean of this distribution is estimated by the reconstructed image and unbiased estimates of the variances can be obtained accurately by applying the methods outlined in [16, 19]. The Fourier reduction detailed in [17, 19] that combines the assumption of relative uniformity of the variances in the observed bins with the properties of the Radon transform is used to assess the correlations. This technique is a computationally elegant implementation of the spatially invariant correlation structure of Carson *et al.* [3].

The above results can be used to suggest an approximate distribution for a dynamic sequence of reconstructed PET scans. The data recorded by the detector over time are independent. Further, the reconstruction of the radio-tracer uptake at any one time-point, does not involve the observations at any other; hence, the reconstructions are themselves independent over time. This gives

Result 1 *The asymptotic distribution of the time-course reconstructed PET sequence $\{\hat{\lambda}^h(t); t = 1, 2, \dots, T\}$ is a Gaussian random field.*

2.2 Synthetic Simulation Approach to Estimating Dispersions

Result 1 implies that for high expected total emissions, the distribution of the time-course reconstructed PET sequence can be approximated by a Gaussian random field. This is used to construct a practical modification to the resampling scheme outlined earlier. The exact implementation is as follows:

1. Obtain a time-course reconstructed image sequence of radio-tracer uptake from the PET study. Also, obtain the variance estimates of the reconstructed pixel values for each of these scans. Approximate the correlations between

the reconstructed pixel values in each scan by the spatially invariant correlation structure developed in [17, 18, 19]. From this reconstructed PET sequence, obtain a functional image of the estimated pixel-wise tissue biologic parameters.

2. Simulate from a Gaussian random field with mean estimated by the above reconstructed time-course sequence. The spatially invariant correlation structure means that Fourier methods can be used in the simulation of correlated multivariate Gaussian realizations (see appendix for details). From each simulated PET sequence, obtain pixel-wise simulated images of the desired biologic parameters.
3. Estimate dispersion of the estimated functional image from this bootstrap sample.

This approach is practical because it eliminates the cumulative computational overhead of performing many reconstruction steps while obtaining resampling estimates of variability.

3 Evaluation of Suggested Strategy

3.1 Diagnostic Checks

Diagnostic checks were performed to evaluate the approximation of the distribution of a reconstructed PET scan by the multivariate Gaussian distribution and a spatially invariant correlation structure at realistic total expected emissions rates. There are two levels of approximation here: (1) appropriateness of the asymptotic Gaussian distributional assumption in a typical PET scan, and (2) assumption of a spatially invariant Fourier correlation structure. Both of these need to be tested. To this end, experiments were performed on a set of simulation PET experiments.

Experiments The model chosen in the diagnostic checks was a version of the Shepp-Vardi-Kaufmann phantom [25] digitized on a 128×128 grid (Figure 3.1a). The sinogram domain had 128×320 distance-angle bins. A sample realization is shown in Figure 3.1b. Evaluations were done over a range of realistic total expected emissions. These were allowed to vary over 9 distinct values (equi-spaced on a \log_2 scale) between 10^4 and 10^6 . This range is comparable to that seen in individual scans in a typical dynamic PET study using the radio-tracer [F-18]-deoxyglucose. For each of these total expected counts, 1000 realizations were generated in the observation domain and reconstructions obtained. The resolution size (FWHM) of the filter for each reconstruction was set so as to provide optimal reconstructions at the corresponding total expected counts. The reconstructions were standardized to have zero mean and unit variance. The reference distribution was the sum of squares of these standardized reconstructed pixel values, where the summation index was over all those pixels that were not

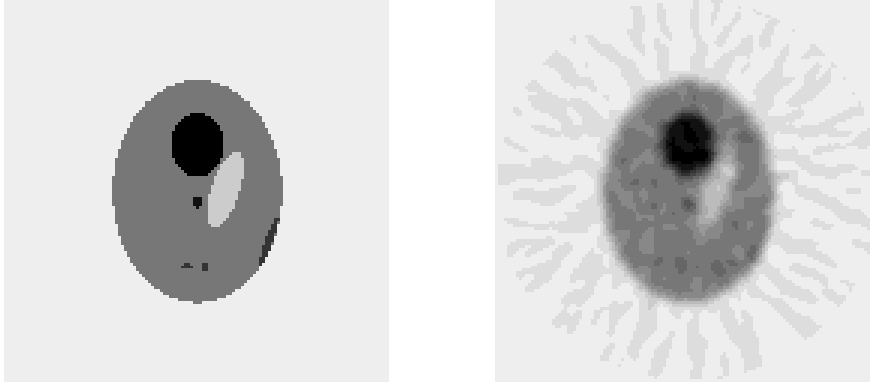


Fig. 1. (a) The Vardi-Shepp phantom used in the simulations. (b) Sample reconstruction.

in the background of the imaging region. The statistic used was

$$W_2 = \sum_{i=1, i \notin \mathcal{B}}^I \frac{[\hat{\lambda}_i^h - \mathbb{E}(\hat{\lambda}_i^h)]^2}{\text{Var}(\hat{\lambda}_i^h)} \quad (2)$$

where \mathcal{B} represents the pixels in the background of the image. The diagnostic checks were performed by comparing the distribution of this statistic W_2 with that obtained by summing up the corresponding squared coordinates of sample realizations generated from a multivariate Gaussian distribution with zero mean and unit variance and the appropriate spatially invariant correlation structure.

Results This section reports the results of our diagnostic checks. The goodness-of-fit for the distribution of W_2 was evaluated both in terms of descriptive plots and analytically. For descriptive analyses, quantile-quantile plots of the test sample were compared with those generated using the reference sample. Linearity in the plots implies agreement with the asymptotic multi-Gaussian distribution.

Figure 2 plots the quantiles of the empirical distribution of W_2 against those obtained from the sample drawn from the reference distribution for the range of counts. The plots are by and large linear and, as expected, the quality of the linear fit improves with increasing count. However, the slope is lower than unity with increasing count rate. This can be explained by the fact that for higher total expected emissions, the optimal bandwidth required in smoothing the reconstructions for consistency is lower and as seen in several studies [3, 17, 19], the dispersions are under-approximated at lower smoothing levels.

To further our understanding of the performance of the diagnostic evaluations, the two-dimensional PET experiments were repeated by fixing the total

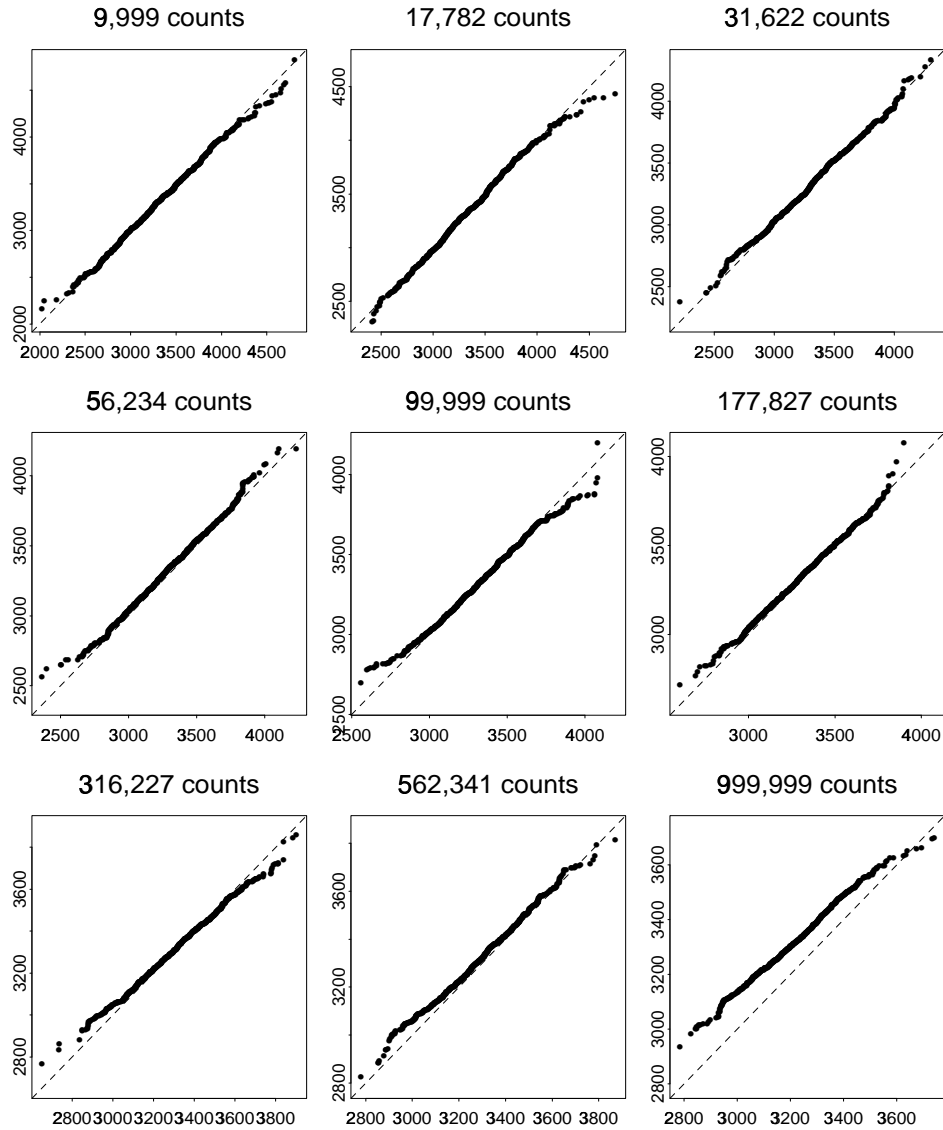


Fig. 2. Quantile-quantile plots of the empirical distribution of W_2 generated from the reference distribution against those obtained from simulations obtained from the model. The asymptotic fit is tested by looking at a range of counts.

expected emissions at the highest level (10^6) and varying the bandwidth over the range of nine corresponding values used in the previous experiments. The plots (not reported here) were generally similar to those in Figure 2. However, at higher bandwidths, the upper quantiles of W_2 were slightly heavier. The slope of the plot went down, away from unity with decreasing bandwidth, thus strengthening our view that it is the under-approximated dispersions for lower bandwidths that made the diagnostic suspect in the previous experiments. These experiments again underline the need for improved schemes for approximating dispersions in reconstructed PET scans; however, the multi-Gaussian distributional approximation to a reconstructed PET scan seems reasonable.

3.2 Variance Estimation in Parametric Images

Mixture Models The mixture analysis approach [20, 22] to parametric imaging is one of many methods suggested in the literature. Let $\lambda_i(t)$ represent the true source distribution in the t 'th time-bin at the i 'th pixel in the PET imaging domain. The vector $\lambda_i(\cdot) = \{\lambda_i(t); t = 1, 2, \dots, T\}$ is called the true *time-activity curve* (TAC) at the i 'th pixel. A K -component mixture model represents the i 'th pixel TAC as a weighted average of K underlying curves (sub-TACs) ξ_k , $k = 1, 2, \dots, K$.

$$\lambda_i(t) = \sum_{k=1}^K \pi_{ik} \xi_k(t) \quad (3)$$

where the mixing proportions $\{\pi_{ik}; k = 1, 2, \dots, K\}$ lie in the K -dimensional simplex. The physical basis for such a representation is that the sub-TACs (ξ 's) correspond to the different tissue types represented in the image and the underlying π_i 's indicate the anatomic tissue composition of the underlying pixel.

Parametric imaging maps the metabolic parameter of interest, ϑ , at each pixel in the image. The mixture analysis approach fits the metabolic parameter $\vartheta^{(k)}$ to each tissue sub-TAC $\xi_k(\cdot)$ and following (3) regards each pixel biologic parameter as a composition of the component tissue parameters,

$$\vartheta_i = \sum_{k=1}^K \pi_{ik} \vartheta^{(k)} \quad (4)$$

Estimation Algorithms For functional imaging, the data are a time-course sequence of reconstructed PET scans $\hat{\lambda}^h = \{\hat{\lambda}^h(t); t = 1, 2, \dots, T\}$. The number of tissue types, K , the sub-TACs $\xi_k(\cdot)$, and the mixing proportions π_{ik} 's have to be determined. K is obtained from anatomic considerations or through clustering or other sophisticated algorithms [20, 22]. Estimation of ξ 's and π 's is usually done alternately to fit the model,

$$\hat{\lambda}_i^h(t) \sim \sum_{k=1}^K \pi_{ik} \xi_k(t); \quad t = 1, 2, \dots, T. \quad (5)$$

The problem of estimating ξ 's, given the π 's, is a low-dimensional problem and usually robust to the choice of the estimation method. On the other hand, the dimensionality of the π_{ik} 's is high and so the estimation problem is delicate. Many methods have been proposed: among them is a quadratic (weighted) least-squares algorithm which constrains π_{ik} 's to belong to the K -dimensional simplex.

The tissue metabolic parameters $\vartheta^{(k)}$'s are estimated from the $\xi_k(\cdot)$'s and the pixel metabolic parameters are estimated following (4):

$$\hat{\vartheta}_i = \sum_{k=1}^K \hat{\pi}_{ik} \hat{\vartheta}^{(k)} \quad (6)$$

Experiments Experiments were conducted to assess the performance of the suggested approach for estimating the pixel-wise variances of the functional parameters, ϑ 's. Since it is not possible, with existing computational power, to estimate/compute the true variances in a two-dimensional PET setup needed for purposes of comparison, evaluations were done in a simplified one-dimensional deconvolution setting with projection characteristics as described in [21]. A 6-component mixture model was specified. Since as explained earlier, most of the variability is in the estimation of the mixing proportions, the component sub-time activity curves ξ 's (and hence $\vartheta^{(k)}$'s) were known. The relationship between

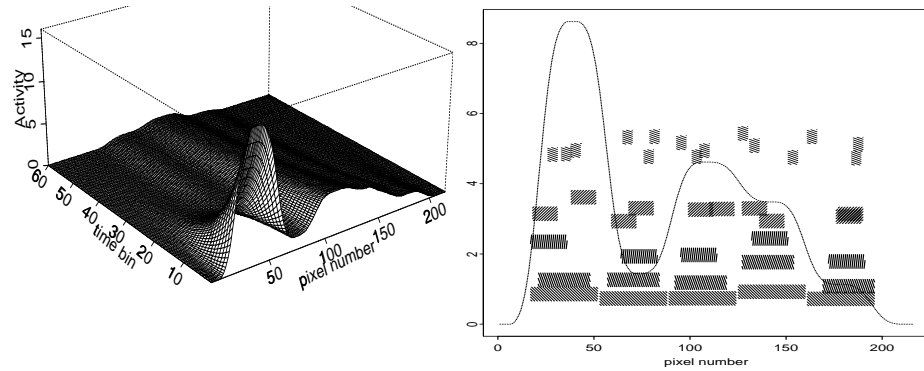


Fig. 3. (a) Perspective plot of the source distribution $\lambda(\cdot)$ used in the experiments. (b) The selected regions (ROI) (shaded bars) and the true source distribution at the fifth time-point (broken line). Size of the shaded bars is proportional to the ROI size.

ξ_k 's and $\vartheta^{(k)}$'s was specified by the equation

$$\xi_k(t) = \vartheta^{(k)} \exp\{-h_k t\}; \quad k = 1, 2, \dots, 6. \quad (7)$$

This implies that $\vartheta^{(k)} = \xi_k(0)$. This is called the “amplitude parameter”. h_k is another functional parameter (the “half-life”) but this parameter was not of

interest in this experiment. The source distribution $\lambda(\cdot)$ (Figure 3a) was specified using (3) with mixing proportions (π_{ik} 's) that were blurred step functions [5]. The target functional parameter was defined using the π 's and the $\vartheta^{(k)}$'s in (4).

Time activity curves over 60 time-points were reconstructed at 216 bins (pixels) from realizations of an inhomogeneous Poisson process in the observation domain [5]. The reconstructions were smoothed by a Gaussian kernel with bandwidth preset to correspond to smoothing parameters that are reasonable for the given total expected emissions. The π_{ik} 's were estimated from $\hat{\lambda}^h(\cdot)$ and used to obtain $\hat{\vartheta}$'s.

1000 simulated reconstructions of the TAC were obtained by simulating the observed process and $\hat{\vartheta}$'s were extracted from each $\hat{\lambda}^h(\cdot)$. Sample pixel-wise standard deviations of these $\hat{\vartheta}_i$'s were assumed to be the “ground truth” in our performance evaluations.

Realizations were simulated from the approximate multi-Gaussian model for the estimated TACs $\hat{\lambda}^h(\cdot)$. Bootstrap samples of $\hat{\vartheta}$'s were obtained as outlined in Section 2.2 and standard deviations calculated. The experiment was done with bootstrap sample sizes $m=10, 30$ and different total expected emissions and replicated 500 times in order to study the distributional properties of these bootstrapped standard deviations.

The above experiment was performed using an extension of the simulation approach in [11]. Sample data sets were simulated in the observation domain followed by reconstruction and mixture analysis to obtain sample parametric data sets from where variances of the parameters were estimated. This simulation strategy is impractical to implement in the two-dimensional PET context; however, in the one-dimensional experiments, it can be used as a benchmark for our synthetic resampling scheme, indicating the performance of our strategy when applied to PET.

The suggested modified simulation method for estimating dispersions was also evaluated for estimating the covariances. This was done in terms of the ability to estimate the variances of the mean functional parameter in 40 homogeneous regions of sizes that ranged from 6 to 36 pixels. The locations of these regions are shown in Figure 3b. The true intensity of the source distribution at the fifth time-point is shown in the background. As before, the experiments were performed for different ranges of counts as well as different bootstrap sample sizes.

Results The results of the experiments conducted to evaluate the modified bootstrap approach are presented here. Figure 4a is a plot of the functional parameter — the “amplitude” — along with a sample estimate obtained using mixture analysis. The suggested method was evaluated in terms of its ability to assess the variance of this estimate. The percent relative absolute bias, averaged over pixels ranged from around 4–5% for all count rates and bootstrap sample sizes. Figure 4b shows a set of pixel-wise bootstrapped standard deviation estimates (points). Here the bootstrap sample size, $m=10$. The “true” standard deviation is shown by means of the broken line in Figure 4b. This was estimated

from replicating the experiment 1000 times. The standard deviations were high in regions where the value of the parameter was high. The bootstrapped standard deviation estimates were post-processed by smoothing with the variable-span smoother of Friedman [7] which uses a local cross-validation scheme to adaptively estimate the resolution size of the smoothing filter. The smoothed estimate (Figure 4b, bold line) gave a better fit. Variability of the estimates was measured by the average, over pixels, of the mean percent absolute error in estimated standard deviation. Table 1 summarizes the bias and the variability

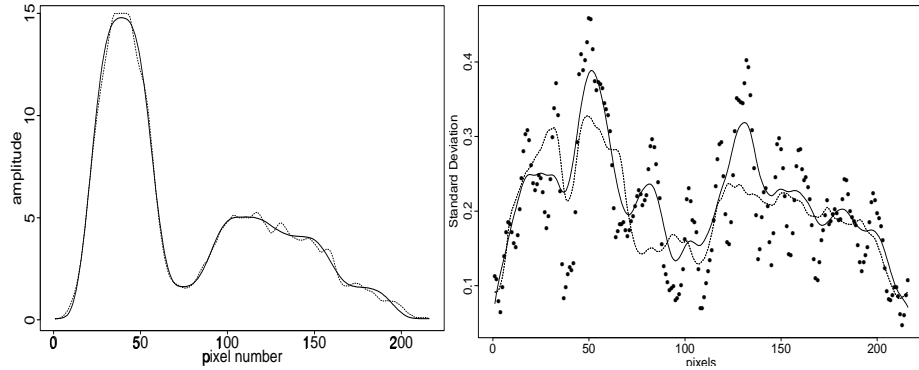


Fig. 4. (a) true amplitude (broken line) and a sample estimate (bold line); (b) true pixel-wise standard deviation (broken line) of the estimated amplitude and its unsmoothed (points) and smoothed (bold line) estimates (10 bootstrap replications).

measures of the estimated bootstrap standard deviations for both the synthetic

Table 1. Bias and variability measures for smoothed bootstrap standard deviation estimates over different total expected counts and bootstrap sample sizes. The bias measure is the percent relative bias averaged over pixels and the variability measure is the mean relative percent absolute error in estimating standard deviations averaged over pixels. Corresponding measures for unsmoothed estimates are in parenthesis. The measures in the left block were obtained using the synthetic resampling approach while those in the right block were obtained using the usual resampling strategy.

Counts ($\times 10^5$)	Bias		Variability		Bias		Variability	
	10 rep	30 rep	10 rep	30 rep	10 rep	30 rep	10 rep	30 rep
1.02	4.6	4.8	17.3	14.0	4.8	4.9	17.4	13.9
	(5.6)	(3.7)	(27.7)	(21.6)	(5.2)	(3.8)	(27.7)	(21.4)
2.05	5.1	5.1	16.1	12.9	5.0	5.0	16.2	12.9
	(3.8)	(5.4)	(27.6)	(21.3)	(5.2)	(4.1)	(27.5)	(21.4)
4.10	5.1	4.9	15.5	12.3	4.8	5.1	15.4	12.3
	(5.3)	(3.7)	(27.3)	(21.0)	(5.1)	(3.7)	(27.4)	(20.9)

resampling approach (left block) as well as the usual resampling strategy (right

block). There is virtually no difference between either method, suggesting good performance of our approximate resampling scheme for variance estimation of parametric images. Further, the percent relative absolute biases are not altered appreciably as a result of the smoothing; however, the variability measures are considerably improved. The bias and variability rates do not differ appreciably

Table 2. Bias and variability measures for estimated standard deviations of mean estimated functional parameters over regions and different bootstrap sample sizes. Bias and variability measures are similar to those in Table 1. The reported percentages are averaged over regions of the same size.

ROI size (pixels)	Bias			Variability		
	<i>10 rep</i>	<i>20 rep</i>	<i>30 rep</i>	<i>10 rep</i>	<i>20 rep</i>	<i>30 rep</i>
6	4.5	2.69	3.09	25.88	21.61	19.91
14	3.64	2.54	2.40	21.54	16.51	14.56
20	3.91	2.68	2.52	20.34	14.69	13.11
28	3.55	2.19	1.66	19.92	13.79	11.48
36	3.18	2.02	2.00	19.52	13.79	11.66

for different total expected counts, for the unsmoothed estimates. This points suggests that the unsmoothed estimators. As expected, the error rates decrease with increasing bootstrap sample size.

The errors in estimating standard deviations of the estimated mean functional parameter over the 40 homogeneous regions are presented in Table 2. The variability measures decreased with increasing size of region; a corresponding, albeit slight, phenomenon was also reported for the bias measures. Since summing over larger regions tends to have a smoothing effect, this is expected. However, since the variability measures are still high, this suggests the need for post-processing the estimates.

4 Discussion

The main contribution of this paper is a practical approach to variability assessment in parametric images obtained from dynamic sequences of reconstructed Positron Emission Tomography (PET) scans. The approach hinges on the approximation of the distribution of the reconstructed PET sequence by a Gaussian random field. The dispersions are specified by the Fourier methods outlined in Maitra [17]. Diagnostic checks were performed to test the validity of our suggestion, in the context of simulation PET experiments. Further, a one-dimensional analogue of the PET reconstruction problem was used to evaluate the performance of the approach in estimating the variances of the estimated parameters, with encouraging results. Though the focus has been the estimation of pixel-wise variances of parametric images using the mixture analysis of O’Sullivan [20, 22], the technique is general enough to be applied to variance assessment in parametric images obtained by approaches other than mixture analysis.

A number of issues remain to be addressed. As seen in the experiments, the estimation process can be improved by post-processing the estimated variances. The crude smoothing algorithm we have used does not perform well in the presence of correlated coordinates, which is very likely in our case. Hence, the obtained error rates may potentially be decreased by a more sophisticated choice of smoothing parameter. Another question of interest is determining the number of bootstrap samples. Further, the diagnostic tests indicate that there is need for better dispersion estimation procedures, especially at lower bandwidths. An attraction of the Fourier method of estimating correlations is the computational efficiency in generating correlated data — such an approach is not necessarily possible even in the one-dimensional model where we have accurate correlation computation procedures [16, 17]. Hence, there is need for developing better dispersion estimation procedures, and also efficient simulation procedures that can generate data with similar correlation structures. Another issue is the incorporation of correction factors that are routinely applied to the PET reconstructions in order to account for detector geometry and other effects. Since the ultimate goal of this exercise is to develop practical inference tools to guide diagnostic decisions, these issues will have to be addressed. With the increasing use of three-dimensional scanners, modest moves are beginning to be made in the direction of using these reconstructions for quantitative purposes. Extending the suggested technique to such settings would be invaluable for diagnosis. Thus, while this seems a promising new technique towards variability estimation in functional images, a number of questions remain to be investigated. To this end, a promising beginning with great potential can be said to have been made.

APPENDIX: FOURIER SIMULATION METHODS

In matrix notation, the reconstruction equation can be expressed as

$$\hat{\lambda}^h = S_h(K'K)^{-1}K'y \quad (8)$$

where y is the corrected projection data, K is the discretized version of the Radon transform, and S_h represents the smoothing operation of resolution size (FWHM) h that is applied to the raw reconstructions in order to obtain acceptable solutions [21]. Under the assumption of relative uniformity of variances of the observed y 's, it can be shown [17, 18, 19] that the reconstruction $\hat{\lambda}^h$ has a spatially invariant correlation structure given by

$$\text{Corr}(\hat{\lambda}_i^h, \hat{\lambda}_j^h) = \frac{C_h(|i-j|)}{C_h(0)}, \quad (9)$$

where $\mathcal{Y} = \{C_h(0), C_h(1), \dots, C_h(I)\}$ is the first row of the approximately Fourier matrix $S_h(K'K)^{-1}S_h$.

Let $Z = \{Z_1, Z_2, \dots, Z_I\}$ be independent standard Gaussian random variables. Denote \check{Z} and $\check{\mathcal{Y}}$ as the corresponding Fast Fourier transforms of Z and \mathcal{Y} , respectively. $\check{\mathcal{Y}}$ is real-valued and positive, and so is $\check{\Psi} = \sqrt{\check{\mathcal{Y}}}$. Defining B_h as the

the matrix formed by the rows obtained by permuting the inverse Fourier transform of $\check{\Psi}$, we get $B_h B_h' = S_h (K' K)^{-1} S_h$. Let $X = \{X_1, X_2, \dots, X_I\} = B_h Z$. Then X can be readily obtained from Z by discrete convolution with Ψ . This step can be achieved via Fast Fourier transforms. Further, X forms a set of correlated zero-mean, unit-variance Gaussian variables with the desired correlation structure. Let $R_i = \hat{\lambda}_i^h + \hat{\tau}_i X_i$, where $\hat{\tau}_i^2$ is the variance estimate of $\hat{\lambda}_i^h$ detailed in [17, 18, 19]. Then $R = \{R_1, R_2, \dots, R_I\}$ is a realization from the asymptotic distribution of $\hat{\lambda}$. The realizations are readily simulated because of the Fast Fourier Transforms used in obtaining correlated realizations.

Acknowledgements

I would like to thank Professor Finbarr O'Sullivan, my dissertation advisor in the Department of Statistics at the University of Washington, for introducing me to this problem and for the many hours of helpful advice and invaluable insights that I have received from him. Some of the routines used in the one-dimensional experimental evaluations were written by Kingshuk RoyChoudhury of the Department of Statistics at the University of Washington: his help is gratefully acknowledged.

References

1. Blomqvist, G., "On the Construction of Functional Maps in Positron Emission Tomography", *J. Cereb. Blood Flow and Metab.*, 4:629-32, 1984.
2. Blomqvist, G., Eriksson L., and Rosenqvist G., "The Effect of Spatial Correlation on Quantification in Positron Emission Tomography" *Neuroimage*, 2:2, 1995.
3. Carson, R. E., Yan, Y., Daube-Witherspoon, M. E., Freedman, N., Bacharach, S. L. and Herscovitch, P., "An Approximation Formula for the Variance of PET Region-of-Interest Values", *IEEE Trans. Med. Imag.*, 12:240-50, 1993.
4. Cunningham, V. J., and Jones, T., "Spectral Analysis of Dynamic PET Studies", *J. Cereb. Blood Flow and Metab.*, 13:15-23, 1993.
5. Choudhury, K. R. and O'Sullivan, F., "A Statistical Examination of FBP and ML for Estimating Mixture Models from Dynamic PET Data", *1995 IEEE Nucl. Sci. Symp. and Med. Imag. Conf. Record*, 3:1237-1241, 1995.
6. Efron, B., "The Jackknife, the Bootstrap and Other Resampling Plans", SIAM, 1982.
7. Friedman, J. H., "A Variable Span Smoother", *Tech. Rep. No. 5, Lab. for Comp. Stat., Dept. of Stat., Stanford Univ., Stanford, CA*, 1984.
8. Friston, K. J., Frith, C. D., Liddle, P. F., and Frackowiak R. S., "Comparing Functional (PET) Images: The Assessment of Significant Change", *J. Cereb. Blood Flow Metab.*, 11:690-99, 1991.
9. Gjedde, A., "High- and Low-affinity Transport of Glucose from Blood to Brain", *J. Neurochem.*, 36:1463-71, 1981.
10. Gjedde, A., "Calculation of Cerebral Glucose Phosphorylation from Brain Uptake of glucose analogs in vivo: a re-examination", *Brain Res. Rev.*, 4:237-74, 1982.
11. Haynor, D. R. and Woods, S. D., "Resampling Estimates of Precision in Emission Tomography", *IEEE Trans. Med. Imag.*, 8:337-43, 1989.

12. Herholz, K. and Patlak, C. S., "The Influence of Tissue Heterogeneity on Results of Fitting Nonlinear Model Equations to Regional Tracer Uptake Curves. With an Application to Compartmental Models used in Positron Emission Tomography", *J. Cereb. Blood Flow Metab.* 11:10-24, 1991.
13. Herholz, K., "Non-stationary Spatial Filtering and Accelerated Curve-fitting for Parametric Imaging with Dynamic PET", *Eur. J. Nucl. Med.*, 14:477-84, 1988.
14. Heiss, W. D., Kessler, J., Karbe, H., Fink, G. R., and Pawlik, G., "Cerebral Glucose Metabolism as a Predictor of Recovery from Aphasia in Ischemic Stroke", *Arch. Neurol.*, 50:958-64, 1993.
15. Heiss, W. D., Kessler, J., Slansky, I., Mielke, R., Szelies, B., and Herholz, K., "Activation PET as an Instrument to Determine Therapeutic Efficacy in Alzheimer's Disease", *Ann. N. Y. Acad. Sci.*, 695:327-31, 1993.
16. Maitra, R. and O'Sullivan, F., "Estimating the Variability of Reconstructed PET Data : A Technique Based on Approximating the Reconstruction Filter by a sum of Gaussian kernels", *1995 IEEE Nucl. Sci. Symp. and Med. Imag. Conf. Record*, 3:1411-14, 1995.
17. Maitra, R., "Variability Estimation in Linear Inverse Problems", *Ph. D. dissertation*, Department of Statistics, University of Washington, 1996.
18. Maitra, R., "Estimating Precision in Functional Images", *J. Comp. Graph. and Stat.*, 6:1:1-11, 1997.
19. Maitra, R. and O'Sullivan, F., "Variability Assessment in PET and Related Generalized Deconvolution Models", *J. Amer. Stat. Assoc.*, submitted, 1997.
20. O'Sullivan, F., "Imaging Radiotracer Model Parameters in PET : A Mixture Analysis Approach", *IEEE Trans. Med. Imag.*, 12:399-412, 1993.
21. O'Sullivan, F., Pawitan, Y. and Haynor, D., "Reducing Negativity Artifacts in Emission Tomography: Post-Processing Filtered Backprojection Solutions", *IEEE Trans. Med. Imag.*, 12:653-663, 1993.
22. O'Sullivan, F., "Metabolic Images from Dynamic Positron Emission Tomography studies", *Stat. Meth. in Med. Res.*, 3:87-101, 1994.
23. Patlak, C. S., Blasberg, R. G., and Fenstermacher, J. D., "Graphical Evaluations of Blood-to-brain Transfer Constants from Multiple-time Uptake Data", *J. Cereb. Blood Flow Metab.* 3:1-7, 1983.
24. Schmidt, K., Miles, G. and Sokoloff, L., "Model of Kinetic Behavior of Deoxyglucose in Heterogeneous Tissues in Brain: a Reinterpretation of the Significance of Parameters fitted to Homogeneous Tissue Models", *J. Cereb. Blood Flow Metab.* 11:10-24, 1991.
25. Vardi, Y., Shepp, L. A. and Kaufman, L. A., "Statistical model for Positron Emission Tomography", *J. Amer. Statist. Assoc.*, 80:8-37, 1985.
26. Worsley, K. J., Evans, A. C., Marrett, S. and Neelin, P., "A Three-dimensional Statistical Analysis for CBF Activation Studies in Human Brain", *J. Cereb. Blood Flow Metab.*, 12:900-18, 1992.